Cold magnetically trapped ^2D_g scandium atoms. II. Scattering dynamics

Tijs Karman and Gerrit C. Groenenboom*

Theoretical Chemistry, Institute for Molecules and Materials, Radboud University Nijmegen, Nijmegen, The Netherlands

(Received 27 July 2014; published 5 November 2014)

The binary collision dynamics of $^2D_{g,3/2}$ ground state scandium atoms is studied from first principles. We employ 30 coupled diabatic *ab initio* potentials in a coupled-channels study of the scattering dynamics of cold and ultracold scandium atoms in external magnetic fields. Due to the long-ranged magnetic dipolar interaction, the field dependence of the cross section does not follow the threshold laws derived by Volpi and Bohn [Phys. Rev. A **65**, 052712 (2002)]. In the field-free case, the near-threshold cross section is independent of the collision energy, and hence the cross section does not follow the well-established Wigner threshold laws. The observed threshold behavior is explained in the Born approximation. For energies above 1 μK, inelastic collisions are driven by the anisotropic nonrelativistic electronic interaction. For energies below 100 μK, the ratio of elastic-to-inelastic collisions is likely to be favorable for evaporative cooling. Both anisotropy in the long-range interaction and in the short-range potential contribute to large cross sections for inelastic collisions at higher energies and lead to a small ratio of elastic-to-inelastic collisions. This is in agreement with the large rates for Zeeman relaxation of submerged-shell atoms observed experimentally. The effect of the uncertainty in the *ab initio* potential is sampled by scaling the reduced mass and is found to have little influence on the conclusions drawn from this work.

DOI: 10.1103/PhysRevA.90.052702 PACS number(s): 34.50.Cx

I. INTRODUCTION

Experiments on ultracold magnetically trapped atoms and Bose-Einstein condensates are performed mainly with alkali metals [1–3]. Atoms which possess nonzero electronic orbital angular momenta are more difficult to cool to ultracold temperatures [4]. The reason is that for such atoms, the electronic interaction is anisotropic [5]. These anisotropic interactions drive Zeeman relaxation, which leads to heating of the sample and loss of atoms from the magnetic trap.

It has been proposed that the interaction anisotropy may be suppressed for so-called submerged-shell atoms [6,7]. These are atoms with an open subshell that contributes electronic angular momentum, which is screened by a filled subshell of higher principal quantum number. The suppression of angular momentum changing collisions was observed to be efficient for scattering between helium and titanium [8–10], as well as for helium-erbium and helium-thulium collisions [4]. However, scattering of pairs of erbium or thulium atoms leads to unexpectedly large inelastic cross sections [4]. The suppression of reorientation of angular momentum in collisions with rare gas atoms has been explained theoretically [10]. To our knowledge, no theoretical explanation exists for the large inelastic rates found for collisions of pairs of submerged-shell atoms.

In this paper, we present coupled-channels calculations for collisions of scandium atoms. We consider scandium as a model system for submerged-shell atoms, as it is the lightest element of this class of atoms. Scandium has a $^2D_{g,3/2}$ ground state with an $[\mathrm{Ar}]4s^2 3d^1$ configuration. The anisotropy due to the open $3d$ shell is screened by the outer $4s$ electrons. We use the *ab initio* interaction potentials reported in the companion paper [11]. Short-range potentials were calculated using second-order n-electron valence state perturbation theory (NEVPT2). The first-order long-range interaction has been determined at the complete active space self-consistent field level. Long-range dispersion coefficients was determined from frequency-dependent polarizabilities of the atoms calculated using time-dependent density functional theory.

We use the diabatic representation proposed in Ref. [5], which describes the general theory of collisions of open-shell atoms. This theory has previously been applied to the collision of P-state atoms [12–14]. The interaction of P-state atoms can be considered a special case, since each adiabatic state of the dimer can be assigned a definite asymptotic total electronic orbital angular momentum, L. For atoms with orbital angular momentum $L_A \geqslant 2$, this is no longer the case, and in that sense, the present work can be considered the first application of the general theory of Ref. [5]. To the best of our knowledge, calculations for interacting $L_A \geqslant 2$ state atoms have only been performed using model potentials. See, for example, Ref. [15], which describes Zeeman relaxation of dysprosium atoms, using a universal single-channel scattering model and a long-range dispersion potential determined from experimental atomic energy levels. Feshbach resonances in elastic scattering from the high-field seeking states of ultracold dysprosium atoms have been also been investigated using coupled-channels theory and the same model potential [16].

For the special case of collisions between rare gas and ^2P-state atoms, the spin-orbit coupling is known to play a major role in the suppression of interaction anisotropy [17,18]. The reason is that $j = 1/2$ state atoms are not coupled by anisotropic components of the interaction, whereas atoms in the $j = 3/2$ state are. Spin-orbit driven suppression of interaction anisotropy is not expected to play a major role for the interaction of two ^2D-state atoms, as atoms in either spin-orbit state, $j = 3/2$ or $j = 5/2$, interact through quadrupole-quadrupole coupling and anisotropic dispersion [5,19]. Atoms in the $j = 3/2$ ground state are shielded only from the highest rank spherical tensor contributions to the short-range

*gerritg@theochem.ru.nl

interaction. Shielding from these contributions is a minor effect, as it is shown in this paper that even completely turning off the short-range anisotropy is insufficient to significantly increase the ratio of elastic-to-inelastic cross sections.

This article is organized as follows. In Sec. II we discuss the scattering theory including the interactions that we consider, the channel basis, symmetry aspects, and the near-threshold energy and magnetic field dependence of the scattering cross sections. Section III discusses the numerical implementation of the scattering calculation. In Sec. IV we present the results for scattering in field-free space and in external magnetic fields. We find that the interaction anisotropy leads to large inelastic rates. The main mechanism for relaxation in the ultracold limit is determined to be magnetic dipolar coupling. For energies above 10^{-6} K, inelastic collisions are driven by anisotropic nonrelativistic electronic interactions, rather than by the magnetic dipolar coupling. Concluding remarks are given in Sec. V.

II. THEORY

A. Atomic Hamiltonian and quantum numbers

We consider the collision of two scandium atoms, labeled (A) and (B). This section discusses the Hamiltonian and quantum numbers of an isolated atom $(X) = (A)$ or (B). The atomic Hamiltonian is given by

$$\hat{H}^{(X)} = \hat{H}^{(X)}_{\text{elec.}} + \hat{V}^{(X)}_{\text{SO}} + \hat{V}^{(X)}_{\text{Zeeman}}, \tag{1}$$

where $\hat{H}^{(X)}_{\text{elec.}}$ is the nonrelativistic electronic Hamiltonian, $\hat{V}^{(X)}_{\text{SO}}$ is the spin-orbit interaction, and $\hat{V}^{(X)}_{\text{Zeeman}}$ represents the interaction with the external magnetic field. The electronic Hamiltonian is given by

$$\hat{H}^{(X)}_{\text{elec.}} = -\frac{\hbar^2}{2m_e}\sum_i \nabla_i^2 + \frac{e^2}{4\pi\epsilon_0}\left(\sum_{i,j>i}\frac{1}{r_{ij}} - \sum_i \frac{Z_X}{r_{iX}}\right), \tag{2}$$

where $\hbar$ is the reduced Planck constant, m_e is the mass of the electron, e is the elementary charge, ϵ_0 is the vacuum permittivity, r_{ij} is the distance between electrons i and j, and r_{iX} is the distance between electron i and the nucleus of atom X with charge eZ_X. We describe the atoms in Russel-Saunders coupling, with electronic orbital and spin angular momentum quantum numbers, L_X and S_X, total electronic angular momentum, j_X, and corresponding space-fixed projection quantum numbers, M_{L_X}, M_{S_X}, and m_X. Clebsch-Gordan coupling of orbital and spin angular momentum states, $|L_X M_{L_X}\rangle$ and $|S_X M_{S_X}\rangle$, defines the atomic fine structure states as

$$|j_X m_X\rangle = \sum_{M_{L_X} M_{S_X}} \left|L_X M_{L_X}\right\rangle\left|S_X M_{S_X}\right\rangle\left\langle L_X M_{L_X} S_X M_{S_X}\middle| j_X m_X\right\rangle. \tag{3}$$

For ${}^2D_g$ ground-state scandium atoms $L_X = 2$ and $S_X = 1/2$.

The spin-orbit interaction is described by an effective spin-orbit Hamiltonian of the form

$$\hat{V}^{(X)}_{\text{SO}} = A_{\text{SO}}\hat{\mathbf{L}}^{(X)}\cdot\hat{\mathbf{S}}^{(X)}, \tag{4}$$

where $\hat{\mathbf{L}}^{(X)}$ and $\hat{\mathbf{S}}^{(X)}$ are the electronic orbital and spin angular momentum operators, respectively, and the value $A_{\text{SO}} = 0.3068$ mE$_\text{h}$ is taken from experiment [20]. The $j_X = 3/2$ ground state and the excited $j_X = 5/2$ level are split by about 168 cm^{-1}. The interaction with a magnetic field in the space-fixed z direction is given by

$$\hat{V}^{(X)}_{\text{Zeeman}} = -\mathbf{B}\cdot\hat{\boldsymbol{\mu}}^{(X)} = -B\hat{\mu}^{(X)}_z, \tag{5}$$

where the magnetic dipole operator is given by

$$\hat{\boldsymbol{\mu}}^{(X)} = -\mu_B(\hat{\mathbf{L}}^{(X)} + g_s\hat{\mathbf{S}}^{(X)}). \tag{6}$$

Here, μ_B is the Bohr magneton and $g_s \approx 2.0023$ is the electron g factor. In magnetic fields, m_X is conserved, but the fine-structure states are mixed. We denote the exact quantum numbers of the atom by n_X and m_X and express the atomic state in terms of the fine-structure states as

$$|n_X m_X\rangle = \sum_{j_X} |j_X m_X\rangle U_{j_X n_X}. \tag{7}$$

The expansion coefficients, $U_{j_A n_A}$, are elements of a unitary matrix that diagonalizes the matrix representation of the atomic Hamiltonian [Eq. (1)] in the space of the coupled angular momentum states [Eq. (3)]. In the limit where the Zeeman interaction is much weaker than the spin-orbit coupling, j_X is an approximately good quantum number, but the degeneracy of its $2j_X + 1$ sublevels is lifted. The energy difference between the sublevels is proportional to m_X and to the magnetic field strength, B.

For atoms in states with $m_X > 0$, the Zeeman energy increases with the magnetic field strength. Atoms in such low-field seeking states can be trapped magnetically. Therefore, cold magnetically trapped scandium atoms will be in the lowest spin-orbit manifold, $n_X = 3/2$, and initially the space-fixed projection quantum number will equal its maximum value, $m_X = 3/2$.

B. Hamiltonian and scattering theory

The collision is described in the center of mass frame, and the total Hamiltonian is given by

$$\hat{H} = -\frac{\hbar^2}{2\mu R}\frac{\partial^2}{\partial R^2}R + \frac{\hat{\ell}^2}{2\mu R^2} + \hat{H}^{(A)}_{\text{elec.}} + \hat{H}^{(B)}_{\text{elec.}} + \hat{V}_{\text{elec.}} + \hat{V}_{\text{SO}} + \hat{V}_{\text{magn.dip.}} + \hat{V}_{\text{Zeeman}}, \tag{8}$$

where R is the interatomic distance, μ is the reduced mass, the operator $\hat{\boldsymbol{\ell}}$ generates the end-over-end rotation of the collision complex, $\hat{H}^{(X)}_{\text{elec.}}$ represents the electronic Hamiltonian of atom $(X) = (A)$ or (B), $\hat{V}_{\text{elec.}}$ represents the Coulomb interaction between atoms (A) and (B), $\hat{V}_{\text{SO}}$ is the spin-orbit coupling, $\hat{V}_{\text{magn.dip.}}$ is the magnetic dipolar coupling, and $\hat{V}_{\text{Zeeman}}$ represents the interaction with magnetic fields.

To describe the nonrelativistic electronic interaction, $\hat{V}_{\text{elec.}}$, we use the diabatic model proposed in Ref. [5]. The use of a diabatic representation is essential as nonadiabatic coupling vanishes only as R^{-1} [21], whereas the energy splitting between the adiabatic states asymptotically vanishes as R^{-5}. The employed model uses a diabatic basis of transformed adiabatic states that asymptotically correspond to space-fixed

atomic states. A fixed transformation between the adiabatic and diabatic representations is assumed, by diagonalizing the asymptotic interaction in the space of asymptotic atomic states. This model is correct at large separation and resolves the singularity of the Hamiltonian. At short separation, residual nonadiabatic coupling between these states exists, but as these states split up in energy, the coupling may be neglected [5].

The interaction with the magnetic field is given by the sum of the Zeeman Hamiltonians for both atoms

$$\hat{V}_{\text{Zeeman}} = \hat{V}^{(A)}_{\text{Zeeman}} + \hat{V}^{(B)}_{\text{Zeeman}}. \tag{9}$$

The magnetic dipole-dipole coupling between the two atoms is treated in Appendix A. We neglect the R dependence of the spin-orbit coupling and assume that this coupling is described by the atomic limit

$$\hat{V}_{\text{SO}} = \hat{V}^{(A)}_{\text{SO}} + \hat{V}^{(B)}_{\text{SO}}, \tag{10}$$

as the sum of an effective spin-orbit Hamiltonian for each atom.

The collision of two atoms is treated with coupled-channels theory. The scattering wave function is expanded in channel functions as

$$|\Psi_j\rangle = \frac{1}{R}\sum_i |\phi_i\rangle F_{ij}(R), \tag{11}$$

where j labels the entrance channel. The coupled-channels equations are solved numerically for the expansion coefficients, $F_{ij}(R)$. In the short range, we use the renormalized Numerov algorithm [22], whereas in the long range, we use the renormalized Airy propagator [23]. The renormalized Airy algorithm efficiently propagates the solution to very large distances, as is required in this work. For the channel basis we use a fully coupled representation

$$\begin{aligned}|\phi_i\rangle &= |(j_A j_B) j_{AB} \ell; JM\rangle \\ &= \sum_{m_A m_B m_\ell m_{AB}} |j_A m_A\rangle |j_B m_B\rangle |\ell m_\ell\rangle \\ &\quad \times \langle j_A m_A j_B m_B | j_{AB} m_{AB}\rangle \langle j_{AB} m_{AB} \ell m_\ell | JM\rangle,\end{aligned} \tag{12}$$

where i is a composite label for $\{L_A, S_A, j_A, L_B, S_B, j_B, j_{AB}, \ell, J, M\}$. The atomic quantum numbers L_X, S_X, j_X, for $X = A, B$, and the corresponding projection quantum numbers have been defined in Sec. II A. The total electronic angular momentum j_{AB} with projection m_{AB} has been obtained by Clebsch-Gordan coupling of the atomic angular momenta, j_A and j_B. The ket $|\ell m_\ell\rangle$ describes the end-over-end rotation of the system. The total angular momentum J with space-fixed projection M is obtained by vector coupling of j_{AB} and ℓ. Matrix elements of all considered interactions in this angular basis are given in Appendix A.

At large separation, we transform to the uncoupled representation

$$\begin{aligned}&|j_A m_A\rangle |j_B m_B\rangle |\ell m_\ell\rangle \\ &= \sum_{J, M, j_{AB}, m_{AB}} |(j_A j_B) j_{AB} \ell; JM\rangle \\ &\quad \times \langle j_A m_A j_B m_B | j_{AB} m_{AB}\rangle \langle j_{AB} m_{AB} \ell m_\ell | JM\rangle.\end{aligned} \tag{13}$$

In the field-free case, these states are eigenfunctions of the asymptotic Hamiltonian, which consists only of spin-orbit coupling. Hence, we can match the wave function to its asymptotic form in this representation:

$$F_{ij}(R) \simeq R\left[h^{(2)}_{\ell_i}(k_i R)\delta_{ij} + S_{ij} h^{(1)}_{\ell_i}(k_i R)\right]. \tag{14}$$

The functions $h^{(1)}_\ell$ and $h^{(2)}_\ell$ are the spherical Hankel functions of the first and second kind, respectively [24]. The labels i and j enumerate the asymptotic basis, and $k_i = \sqrt{2\mu(E-\epsilon_i)}$ is the channel wave number. The channel energy, ϵ_i, is an eigenvalue of the asymptotic Hamiltonian. Scattering cross sections are calculated from the elements of the scattering matrix, S_{ij}, according to

$$\sigma_{\gamma' \leftarrow \gamma} = \frac{\pi}{k^2_\gamma} \sum_{\ell, m_\ell, \ell' m'_\ell} \left|\delta_{\gamma\gamma'}\delta_{\ell\ell'}\delta_{m_\ell m'_\ell} - S_{\gamma' \ell' m'_\ell; \gamma \ell m_\ell}\right|^2, \tag{15}$$

where the internal state is labeled by the composite label $\gamma = \{j_A, m_A, j_B, m_B\}$. Cross sections for processes where the initial and final states are identical are referred to as elastic cross sections, whereas m_A- or m_B-changing collisions correspond to Zeeman transitions. Transitions to excited spin-orbit manifolds, j_A- or j_B-changing collisions, are energetically not accessible in cold collisions.

When a magnetic field is included the uncoupled states [Eq. (13)] are not eigenstates of the asymptotic Hamiltonian

$$\hat{H}_{\text{asymp}} = \hat{V}^{(A)}_{\text{SO}} + \hat{V}^{(B)}_{\text{SO}} + \hat{V}^{(A)}_{\text{Zeeman}} + \hat{V}^{(B)}_{\text{Zeeman}} + \hat{H}^{(A)}_{\text{elec}} + \hat{H}^{(B)}_{\text{elec}}. \tag{16}$$

Therefore, we transform to an asymptotic basis which is related to the uncoupled representation by

$$\begin{aligned}&|n_A m_A\rangle |n_B m_B\rangle |\ell m_\ell\rangle \\ &= \sum_{j_A, j_B} |j_A m_A\rangle |j_B m_B\rangle |\ell m_\ell\rangle U_{j_A n_A} U_{j_B n_B},\end{aligned} \tag{17}$$

where $U_{j_A n_A}$ are elements of the unitary transformation discussed in Sec. II A. Scattering cross sections are determined from Eq. (15) with $\gamma = \{n_A, m_A, n_B, m_B\}$. Again, collisions that preserve m_A and m_B are referred to as elastic, whereas m_A- or m_B-changing collisions correspond to Zeeman transitions. As the Zeeman transitions from the $m_A = n_A$ and $m_B = n_B$ initial states are exothermic, these are also referred to as Zeeman relaxation.

For the extent of the radial grid, we can formulate some minimal requirements. If a magnetic field is present, avoided crossings occur at large separation, and these should be included in the radial grid [25]. The position of these crossings may be estimated from the criterion that the difference between the centrifugal terms for the initial and final states compensates the Zeeman splitting

$$g_j \mu_B B \Delta m_{AB} = \frac{\hbar^2[\ell'(\ell'+1) - \ell(\ell+1)]}{2\mu R^2}. \tag{18}$$

Here ℓ is the angular momentum associated with the end-over-end rotation, and the change in projection quantum numbers is defined as $\Delta m_{AB} = m_A + m_B - m'_A - m'_B$, where unprimed

(primed) quantum numbers refer to initial (final) states. In the lowest spin-orbit manifold, $j = 3/2$ and the Landé g factor $g_j \approx 0.8$, as will be discussed in Sec. II D. In the field-free case, magnetic dipolar relaxation also occurs at long range, and one should propagate past the classical turning point

$$R_c = \sqrt{\frac{\ell(\ell+1)}{2\mu E}}. \tag{19}$$

See Sec. II D for a detailed discussion. For the lowest energies of 10^{-7} K considered in this work, propagation to $5\times10^4\ a_0$ is required.

C. Symmetry constraints

In Appendix B, we consider the action of spatial inversion, $\hat{i}$, and nuclear permutation, $\hat{P}_{AB}$, on the channel functions of Eq. (12). The results are

$$\begin{aligned}
&\hat{i}|(j_A j_B)j_{AB}\ell; JM\rangle \\
&\quad = (-1)^{\ell}|(j_A j_B)j_{AB}\ell; JM\rangle, \\
&\hat{P}_{AB}|(j_A j_B)j_{AB}\ell; JM\rangle \\
&\quad = (-1)^{j_A+j_B-j_{AB}+\ell+n_e}|(j_B j_A)j_{AB}l; JM\rangle,
\end{aligned} \tag{20}$$

where $n_e = 21$ is the number of electrons of the scandium atom. The channel functions are adapted to permutation and inversion symmetry as

$$\begin{aligned}
\left|\phi^{\pm}_{j_A j_B j_{AB}\ell;JM}\right\rangle = \frac{1}{\sqrt{2(1+\delta_{j_A j_B})}}&[|(j_A j_B)j_{AB}\ell; JM\rangle \\
&\mp(-1)^{j_A+j_B-j_{AB}+\ell}|(j_B j_A)j_{AB}\ell; JM\rangle].
\end{aligned} \tag{21}$$

Since these symmetries are conserved, only states with the same permutation symmetry, given by the $\pm$ sign above, and inversion symmetry, given by $(-1)^{\ell}$, are coupled.

The only stable naturally occurring isotope of scandium is ^{45}Sc. This nucleus is a fermion with nuclear spin quantum number $I = 7/2$. As the total wave function should be antisymmetric with respect to the interchange of the two nuclei, the nuclear spin state determines the contribution of symmetric and anti-symmetric channel functions. If all contributing nuclear spin states are symmetric under $\hat{P}_{AB}$, only antisymmetric channel functions occur. This would be the case if all nuclear spins are aligned with the external magnetic field, for example. If the nuclear spins are not aligned, symmetric channel functions also contribute, and the relative weights follow from the nuclear spin statistics for $I = 7/2$.

In the entrance channel, both atoms are in the lowest spin-orbit manifold and have their magnetic moments aligned with the external magnetic field, such that we have $j_A = j_B = 3/2$ and $j_{AB} = j_A + j_B$. Therefore, the symmetrized entrance channel functions exist only for odd parity $[(-1)^{\ell} = -1]$, and antisymmetric entrance channel functions are present only for even parity $[(-1)^{\ell} = 1]$. Thus, if the atoms are prepared in identical internal states, the atoms, which are composite bosons, can collide only through even partial waves, even though the nuclei are identical fermions.

D. Threshold laws

The Wigner threshold laws state that collision cross sections for isoenergetic processes near-threshold depend on the collision energy as

$$\sigma \propto E^{\ell+\ell'}, \tag{22}$$

with ℓ, ℓ' the relative angular momenta in the entrance and exit channels, respectively [26]. For exothermic processes, such as Zeeman relaxation in an external magnetic field, the near-threshold scattering cross sections vary with collision energy as

$$\sigma \propto E^{\ell-1/2}. \tag{23}$$

These threshold laws are independent of the actual interaction mechanism, as long as it operates at finite range [26,27].

Near-threshold elastic collisions in field-free space with even parity will occur through s waves, $\ell = \ell' = 0$, and the cross section will approach a constant value. Zeeman transitions cannot occur through s waves, and the dominant inelastic process will involve one d wave, leading to an inelastic collision cross section proportional to E^2. For odd parity, the lowest partial waves are p waves. Therefore, both elastic and inelastic cross sections are suppressed at least as E^2. In magnetic fields, Zeeman transitions becomes exothermic, and collisions occurring through initial s waves lead to cross sections that diverge as $E^{-1/2}$.

It has been pointed out that the Wigner threshold laws do not apply when long-ranged interactions are present [27,28]. Magnetically trapped atoms necessarily have a magnetic dipole moment, thus long-ranged magnetic dipole interactions are generally present. The near-threshold behavior of magnetic dipolar relaxation of Σ-state diatomic molecules has been derived using the Born approximation in Ref. [29]. These results also apply to the case of magnetically trapped atoms with the minor revision that in this case the magnetic dipole is approximated by

$$\hat{\boldsymbol{\mu}} \approx g_j \mu_B \hat{\mathbf{j}}. \tag{24}$$

The Landé g factor depends on the spin-orbit manifold and can be calculated as

$$\begin{aligned}
g_j &= \alpha_L + g_s \alpha_S, \\
\alpha_L &= \frac{j(j+1) - S(S+1) + L(L+1)}{2j(j+1)}, \\
\alpha_S &= \frac{j(j+1) - L(L+1) + S(S+1)}{2j(j+1)}.
\end{aligned} \tag{25}$$

For scandium we have $L = 2$, $S = 1/2$, and $j = 3/2$ in the lowest spin-orbit manifold. Equations (25) yield $g_j = 0.79954$, which is in good agreement with the experimental value of $g_j = 0.79933$ [20].

We will not repeat the derivation in Ref. [29] but simply state the resulting scattering cross section in the Born

approximation

$$\sigma^{\mathrm{BA}}_{\gamma'\leftarrow\gamma} = \frac{15\pi^3\mu^2}{2\hbar^4}(\mu_B g_j \alpha)^4 (2j_A+1) j_A(j_A+1)(2j_B+1) j_B(j_B+1) {\sum_{\ell\ell' m_\ell m'_\ell}}' \left(\frac{k}{k'}\right)^{2\ell-1} (2\ell+1)(2\ell'+1)$$
$$\times \left[\frac{\Gamma\left(\frac{\ell+\ell'}{2}\right)}{\Gamma\left(\frac{\ell'-\ell+3}{2}\right)\Gamma(\ell+3/2)}\right]^2 \left\{{}_2F_1\left[\frac{\ell-\ell'-1}{2}, \frac{\ell+\ell'}{2}, \ell+3/2, \left(\frac{k}{k'}\right)^2\right]\right\}^2 \begin{pmatrix} \ell' & 2 & \ell \\ 0 & 0 & 0 \end{pmatrix}^2$$
$$\times \begin{pmatrix} 1 & 1 & 2 \\ \Delta m_A & \Delta m_B & -\Delta m_{AB} \end{pmatrix}^2 \begin{pmatrix} j_A & 1 & j_A \\ -m'_A & \Delta m_A & m_A \end{pmatrix}^2 \begin{pmatrix} j_B & 1 & j_B \\ -m'_B & \Delta m_B & m_B \end{pmatrix}^2 \begin{pmatrix} \ell' & 2 & \ell \\ -m'_\ell & -\Delta m_{AB} & m_\ell \end{pmatrix}^2. \quad (26)$$

Here, Γ is the Gamma function, ${}_2F_1$ denotes Gauss's hypergeometric function, the quantities in round brackets are Wigner 3-jm symbols, and γ is a composite label for the internal state of the atoms, $|\gamma\rangle = |j_A m_A\rangle|j_B m_B\rangle$. The fine structure constant is given by α, and the differences in projection quantum numbers are defined as $\Delta m_A = m'_A - m_A$, $\Delta m_B = m'_B - m_B$, and $\Delta m_{AB} = \Delta m_A + \Delta m_B$. The wave number of the initial state is given by $k = \hbar^{-1}\sqrt{2\mu E}$, with E the collision energy, and primes denote the final state. The effect of the magnetic field is contained in the wave number of the final state

$$k' = \frac{1}{\hbar}\sqrt{2\mu(E + g_j \mu_B B \Delta m_{AB})}. \quad (27)$$

Equation (26) has been derived in the Born approximation and is expected to be valid for low energy and low magnetic fields. Furthermore, this result applies only to the case where $\ell + \ell' \neq 0$, since otherwise Eq. (12) of Ref. [29] diverges. The prime on the sum serves to remind us that the term with $\ell = \ell' = 0$ is excluded. For fixed $B \neq 0$, Zeeman relaxation is exothermic, and near threshold $k \ll k'$. In this case, the threshold behavior of the cross sections is $\sigma \propto E^{\ell-1/2}$ and $\sigma \propto B^{1/2-\ell}$ [29]. We note that this energy dependence is consistent with the Wigner threshold laws [Eq. (23)], but the magnetic field dependence is different from that derived in Ref. [30].

For zero magnetic field $k = k'$, and the resulting cross section can be obtained as the limit of Eq. (26) for $B \to 0$,

$$\sigma^{\mathrm{BA}}_{\gamma'\leftarrow\gamma} = 1920\pi\mu^2 \left(\frac{g_j \mu_B \alpha}{\hbar}\right)^4 (2j_A+1) j_A(j_A+1)(2j_B+1) j_B(j_B+1) {\sum_{\ell\ell' m_\ell m'_\ell}}' \frac{(2\ell+1)(2\ell'+1)}{[(\ell'-\ell-1)(\ell'-\ell+1)(\ell'+\ell)(\ell'+\ell+2)]^2}$$
$$\times \begin{pmatrix} j_A & 1 & j_A \\ -m'_A & \Delta m_A & m_A \end{pmatrix}^2 \begin{pmatrix} j_B & 1 & j_B \\ -m'_B & \Delta m_B & m_B \end{pmatrix}^2 \begin{pmatrix} \ell' & 2 & \ell \\ 0 & 0 & 0 \end{pmatrix}^2 \begin{pmatrix} \ell' & 2 & \ell \\ -m'_\ell & -\Delta m_{AB} & m_\ell \end{pmatrix}^2$$
$$\times \begin{pmatrix} 1 & 1 & 2 \\ \Delta m_A & \Delta m_B & -\Delta m_{AB} \end{pmatrix}^2. \quad (28)$$

Again, the prime on the sum serves to remind that the term with $\ell = \ell' = 0$ is excluded. In this case, the scattering cross section is independent of the energy, $\sigma \propto E^0$, which is not consistent with the Wigner threshold laws. Apart from a factor k/k', the energy dependence is completely contained in a radial integral of the form

$$\int_0^\infty j_\ell(kR) R^{-3} j_{\ell'}(k'R) R^2 \, dR = \int_0^\infty j_\ell(xk/k') j_{\ell'}(x) x^{-1} \, dx. \quad (29)$$

The functions $j_\ell(x)$ are the spherical Bessel functions of the first kind [24]. In the field-free case $k = k'$, and this integral is independent of energy, leading to a constant cross section. The integrand peaks in the region where the Bessel functions are maximal, i.e., near the classical turning point

$$R_c = \sqrt{\frac{\ell(\ell+1)}{2\mu E}}. \quad (30)$$

In the ultracold limit, $E \to 0$, the classical turning point moves to infinitely large separation, and the Wigner threshold laws are not applicable.

For nonzero magnetic fields, the classical turning point for the final state occurs at finite separation, given by

$$R_c = \sqrt{\frac{\ell'(\ell'+1)}{2\mu g_j \mu_B \Delta m_{AB} B}}. \quad (31)$$

Near the threshold $kR_c \ll 1$, and the spherical Bessel function can be approximated using the expansion

$$j_\ell(x) = x^\ell \frac{2^\ell \ell!}{(2\ell+1)!} + O(x^{\ell+1}), \quad (32)$$

and Eq. (29) is proportional to $(\frac{k}{k'})^\ell$. The cross section is proportional to the product of the square of this integral and a factor k/k', which leads to the scaling $\sigma \propto E^{\ell-1/2}$ and $\sigma \propto B^{1/2-\ell}$, discussed above [29]. Since magnetic dipolar relaxation occurs around the classical turning point, rather than inside the centrifugal barrier, the scaling with the magnetic field does not follow the threshold law of Ref. [30],

$\sigma \propto B^{1/2+\ell'}$, which was derived under the latter assumption. However, for a nonzero magnetic field, the classical turning point occurs at finite separation given by Eq. (31), such that the transition occurs at a finite range, and the energy scaling of the cross section obeys the Wigner threshold laws.

We provide numerical implementations for the evaluation of Eqs. (26) and (28) as MATLAB routines [31]. These are made available in the Supplemental Material [32].

III. NUMERICAL IMPLEMENTATION

The coupled-channels calculations are performed using MATLAB programs [31], which are made available as Supplemental Material [32]. This section discusses the details of the numerical implementation.

A. Calculations without magnetic field

In the field-free case, the total angular momentum, J, is a conserved quantity, and the calculation is performed per J. Furthermore, the calculation is independent of the projection quantum number, M. Calculations for different J use the same radial grid, which is generated beforehand. We use an equidistant grid from 1 to 20 a_0, with a step size of 0.01 a_0, in the short range. Beyond 20 a_0, the radial grid is extended logarithmically, such that the step size doubles every 50 steps but does not exceed 200 a_0.

Then, per total angular momentum, J, we generate two channel bases. One is the primitive basis of Eq. (12); the other is the permutation and inversion symmetry adapted basis of Eq. (21). Then we precompute all angular matrices in the primitive basis, as discussed in Appendix A. We obtain the angular matrices in the symmetry adapted basis by transforming the matrices in the primitive basis with a rectangular transformation.

A detail that deserves additional attention is the computation of the 18-j symbol in the matrix element of the potential. To the best of our knowledge, there is no efficient algorithm to directly compute this 18-j symbol. Therefore, we compute the 18-j symbol in terms of 6-j and 9-j symbols. We use Eq. (A.4.14) of Ref. [33], which is repeated here for completeness:

$$\begin{Bmatrix} k_A & L_A & S_A & & S'_B & L'_B & k_B \\ & & & S & & & \\ L'_A & j_A & & & j'_B & L_B & \\ & & & k_{AB} & & & \\ S'_A & j'_A & j'_{AB} & & j_{AB} & j_B & S_B \end{Bmatrix}$$
$$= \sum_{x_1,x_2} (2x_1+1)(2x_2+1)(-1)^{k_A+k_B+L'_A+L_B+S_B+S'_A-j_B-j'_A+j_{AB}+j'_{AB}} \begin{Bmatrix} j_{AB} & j'_{AB} & k_{AB} \\ x_2 & x_1 & S \end{Bmatrix}$$
$$\times \begin{Bmatrix} L_A & L'_A & k_A \\ L_B & L'_B & k_B \\ x_1 & x_2 & k_{AB} \end{Bmatrix} \begin{Bmatrix} S_A & L_A & j_A \\ S_B & L_B & j_B \\ S & x_1 & j_{AB} \end{Bmatrix} \begin{Bmatrix} S'_B & L'_B & j'_B \\ S'_A & L'_A & j'_A \\ S & x_2 & j'_{AB} \end{Bmatrix}. \quad (33)$$

For efficiency, the double sum over the $3n$-j symbols should not be performed at runtime, but we precompute all the required 18-j and store these on disk. This results in a file of about 100 kB for two ^2D-state atoms.

Then we continue with propagation, during which the W-matrix is constructed by multiplying the angular matrices with the R dependent coefficients and adding the results. First, we use the renormalized Numerov algorithm to propagate across the short range and repeat this step for a number of energies. Then we simultaneously propagate the Q matrices for all energies in the long-range regime. In treating these energies simultaneously, the diagonalizing step in the propagator does not have to be performed repeatedly, which saves computational time.

After propagation, we match to the scattering boundary conditions to obtain the S matrix. The calculation is repeated for all J, and the resulting S matrices are accumulated. Next, we transform to the uncoupled representation for all M and collision energies. Finally, we extract the cross sections for elastic collisions and Zeeman transitions.

B. Calculations with magnetic field

If magnetic fields are included, J is strictly speaking no longer a good quantum number. Since the Zeeman interaction induces only (weak) coupling between states with J quantum numbers that differ at most by 1, it would be a reasonable approximation to neglect these couplings and use J as a good quantum number. We do not make such approximations and treat the Zeeman interaction rigorously. The projection quantum number, M, is conserved, but the calculation is no longer independent of M. The calculation still proceeds by generating a radial grid, as well as primitive and symmetry adapted coupled basis sets, which now contain functions with different J. Angular matrices are calculated as before.

Then, before starting propagation, we numerically determine the asymptotic basis. We first determine the transformation to the uncoupled basis. Next, we consider the asymptotic Hamiltonian for each atom, consisting of its spin-orbit and Zeeman interaction,

$$\hat{H}^{(A)}_{\text{as}} = A_{\text{SO}}/2\left(\hat{j}_A^2 - \hat{L}_A^2 - \hat{S}_A^2\right) + B\mu_B(\hat{L}_{A,z} + g_s\hat{S}_{A,z}), \quad (34)$$

and analogously for atom B. We calculate and diagonalize the matrix representation of this (B-dependent) operator in the basis $\{|j_A m_A\rangle\}$, for fixed m_A and running j_A. The asymptotic basis is determined from the eigenvectors of this matrix, and the channel energies are related to the eigenvalues, using Eq. (17).

After determining the asymptotic basis and channel energies, we determine the total energy from the collision energy and the energy of the initial channel. Then we propagate the solutions of the coupled-channels equations across the radial grid, as in the field-free case. We transform the final Q matrix to the uncoupled representation, and finally to the asymptotic basis. Then we match to the asymptotic boundary conditions, calculate the elastic and inelastic cross sections, and repeat this calculation for all required values of M.

IV. RESULTS

A. Collisions in field-free space

The coupled-channels calculations have been converged to within 1% with respect to the radial grid and the truncation of the angular basis. To this end we used a radial grid that is equidistant with spacing 0.01 a_0 between 1 and 20 a_0, and propagate using the renormalized Numerov method [22]. In the long range, we continue using the renormalized Airy propagator on a logarithmically spaced grid up to 10^3 a_0 for energies $E > 10^{-3}$ K and 5×10^4 a_0 for lower energies [23]. The angular basis is truncated by including only functions with $\ell \leqslant \ell_{\max}$. For calculations with $E < 10^{-3}$ K, the calculation was converged with $\ell_{\max} = 13$, whereas we used $\ell_{\max} = 101$ for energies $E > 10^{-3}$ K.

The cross sections as a function of the collision energy are shown in Fig. 1. The two panels refer to collisions with even and odd parity, respectively. Solid lines correspond to inelastic cross sections, elastic cross sections are shown as dashed-dotted lines. Inelastic cross sections obtained in the Born approximation [Eq. (28)] are shown as dashed lines. For odd parity, also the elastic threshold cross section can be calculated in the Born approximation, and this result is shown as a dotted line. The dashed vertical lines mark three regimes:

(1) For energies $E > 10^{-3}$ K, the short range can be reached classically. In this regime, the magnitude of the elastic and inelastic cross sections is comparable.

(2) In the Wigner regime, at energies between 10^{-3} K and 10^{-6} K, the short range can be reached only by tunneling through the centrifugal barrier. Therefore, the collision cross sections follow the Wigner threshold laws in this regime. Thus, the elastic cross section for even parity becomes constant, whereas the other cross sections are suppressed as $\sigma \propto E^2$, as discussed in Sec. II D

(3) In the Born regime, for energies $E < 10^{-6}$ K, short-range mechanisms are suppressed so heavily that long-ranged magnetic dipolar relaxation becomes dominant. As shown in Sec. II D, this leads to a constant cross section in the limit of zero energy. The results in the Born approximation are shown as dashed lines in Fig. 1. In the ultracold limit, the Born approximation results agree with the coupled-channels calculations to within a few percent.

In the case of odd parity, $(-1)^\ell = -1$, elastic and inelastic collision cross sections are roughly in the same order of magnitude in all three energy regimes. For the even parity case, $(-1)^\ell = 1$, only inelastic collisions are suppressed in the Wigner regime, which increases the ratio of elastic-to-inelastic collisions. Thus, the largest ratio of elastic-to-inelastic collisions can be obtained by preparing all atoms in identical nuclear spin states, such that only even parity collisions occur; see Sec. II C. Therefore, we will focus on the even parity case, $(-1)^\ell = 1$, in the remainder of this work. For energies below 10^{-4} K, the ratio of elastic-to-inelastic collisions is larger than the critical value of 150 [34], and evaporative cooling from such temperatures should be efficient. Unfortunately this is colder than a typical buffer-gas cooled sample [35].

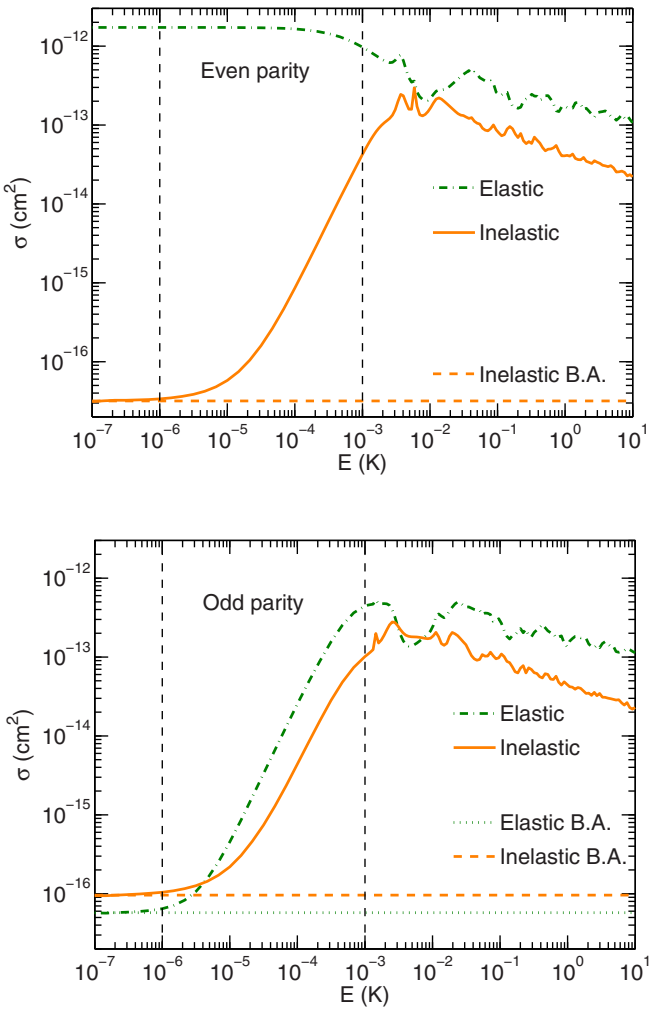

FIG. 1. (Color online) Scattering cross sections as a function of collision energy in field-free space. Solid lines correspond to inelastic cross sections, dashed-dotted lines correspond to elastic cross sections. Results obtained in the Born approximation (BA) are shown as dotted and dashed lines, for elastic and inelastic cross sections, respectively. Vertical dashed lines separate the different regimes, as discussed in the text. The upper panel corresponds to even parity, $(-1)^\ell = 1$, whereas the lower panel corresponds to odd parity, $(-1)^\ell = -1$.

B. Collisions in magnetic fields

Coupled-channels calculations have also been performed including a homogeneous magnetic field. The resulting elastic

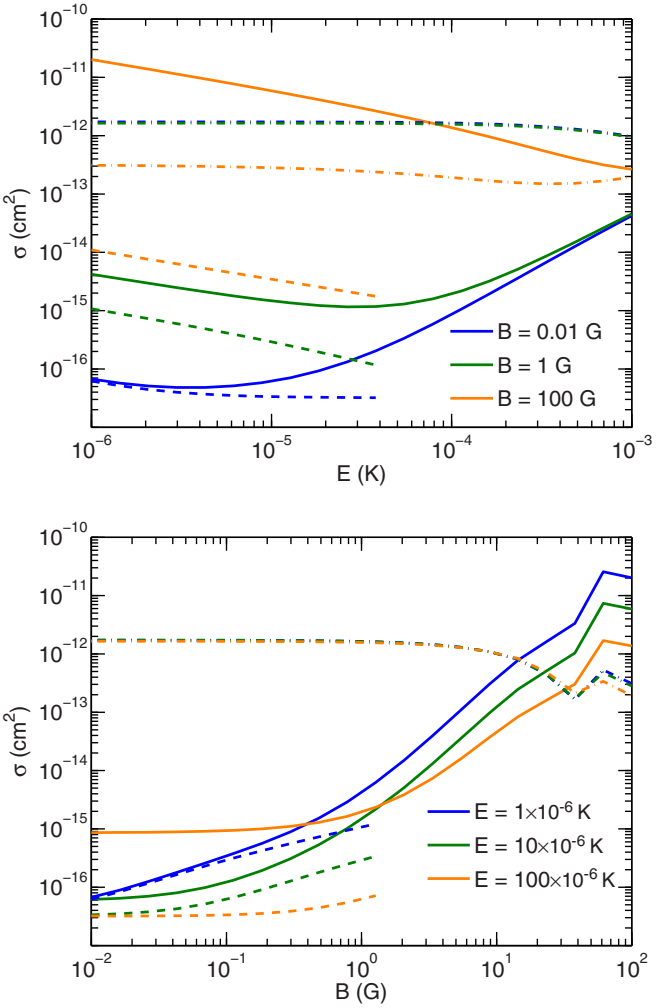

FIG. 2. (Color online) Elastic and inelastic cross sections as a function of the collision energy and magnetic field are shown in the upper and lower panel, respectively. Solid lines correspond to inelastic cross sections, dashed-dotted lines correspond to elastic cross sections, and dashed lines represent results obtained in the Born approximation, respectively.

and inelastic cross sections for the even parity case as a function of collision energy and magnetic field strength are shown in Fig. 2. Solid lines refer to inelastic cross sections, elastic cross sections are shown as dashed-dotted lines, and cross sections obtained in the Born approximation are shown as dashed lines.

In an external magnetic field, Zeeman relaxation becomes an exothermic process. Therefore, the inelastic cross sections are seen to increase with magnetic field strength. For moderate magnetic field strengths of 1 G, the ratio elastic-to-inelastic hardly exceeds the critical value of 150 at any energy.

Quantitative agreement between coupled-channels calculations and the Born approximation is obtained for low energy ($E < 10^{-6}$ K) and low magnetic field strength ($B < 0.1$ G). At higher field strengths, deviations from the results in the Born approximation occur. At a field strength of 100 G, the deviation is larger than three orders of magnitude, and the elastic cross section is also affected.

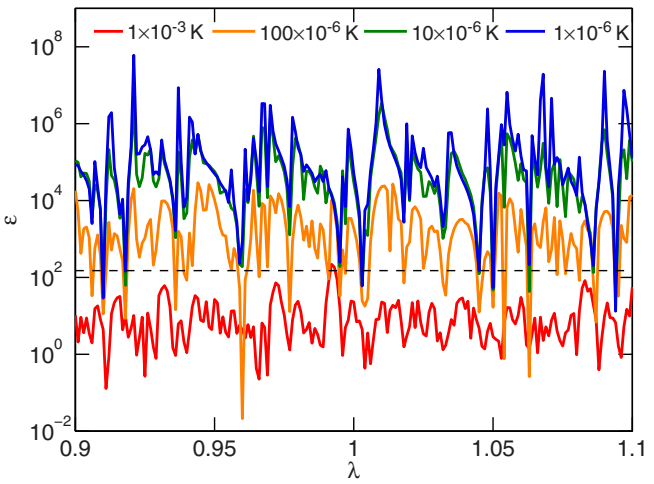

FIG. 3. (Color online) The ratio elastic-to-inelastic, ϵ, as a function of the mass-scaling parameter, λ, for $B = 0$. The dashed line marks the critical value of $\epsilon = 150$.

The differences between the numerically exact coupled-channels calculations and the Born approximation results can be understood in terms of the exothermicity:

$$\Delta E = g_j \mu_B \Delta m_{AB} B. \tag{35}$$

A magnetic field of $B = 1$ G corresponds to an exothermicity of about 5×10^{-5} K, i.e., an energy for which the Born approximation results deviate from the coupled-channels calculations by an order of magnitude in the field-free case, as shown in Fig. 1. Likewise, a field strength of $B = 100$ G corresponds to an exothermicity of about 5×10^{-3} K. At this energy, the Born approximation completely fails in the field-free case, as well. For the lowest field strength of $B = 0.01$ G, the exothermicity is around 5×10^{-7} K, and the Born approximation is accurate for low energies.

C. Sensitivity to the potential

It is well established that scattering cross sections at ultracold energies are highly sensitive to the details of the potential, due to the sensitivity to the position of the least bound state. In order to sample the effect of the uncertainty in the *ab initio* potential, we have scaled the reduced mass by a factor, λ, varying between 0.9 and 1.1. This samples the effect of scattering resonances, as scaling the reduced mass shifts the position of the (quasi-) bound states [36].

The ratio of elastic-to-inelastic collisions, ϵ, as a function of the mass-scaling parameter, λ, for $B = 0$, is shown in Fig. 3. A large number of resonances is observed, owing to the large density of states near zero energy, due to the large reduced mass and deep potential well. For energies below 10^{-4} K, ϵ exceeds the critical value, reasonably independent of λ, and evaporative cooling from such temperatures will be efficient. For energies of 10^{-3} K, ϵ is below the critical value 150, irrespective of λ.

D. Mechanism of Zeeman relaxation

In order to identify the main mechanism for the collisional reorientation of the magnetic moments, we have repeated

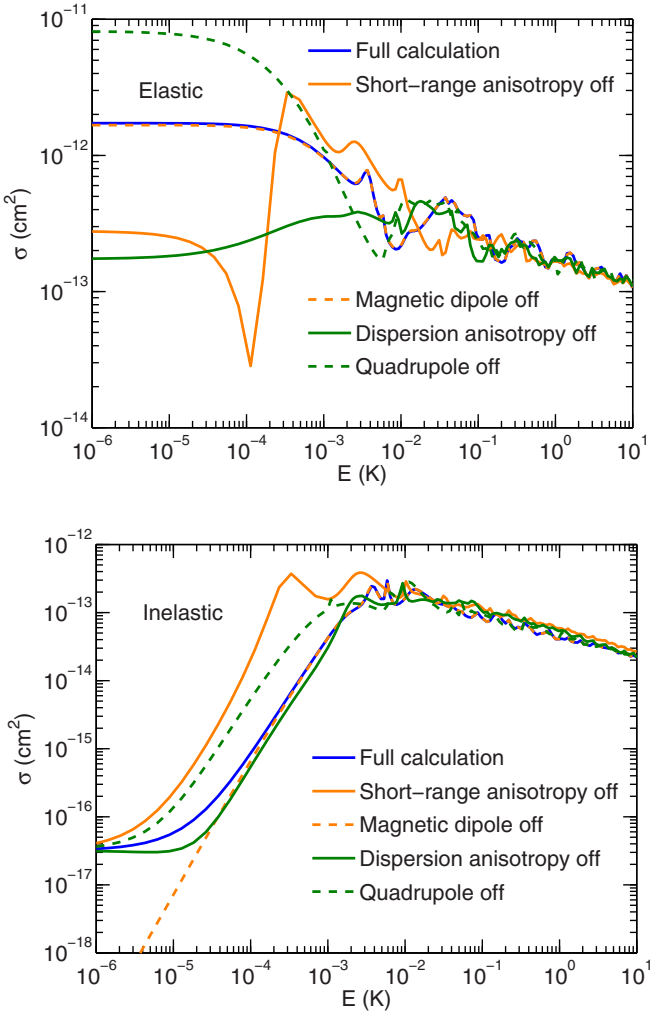

FIG. 4. (Color online) Scattering cross sections as obtained when turning off a single anisotropic interaction for $B = 0$. The top panel shows the elastic cross section, and the bottom panel shows the inelastic cross sections.

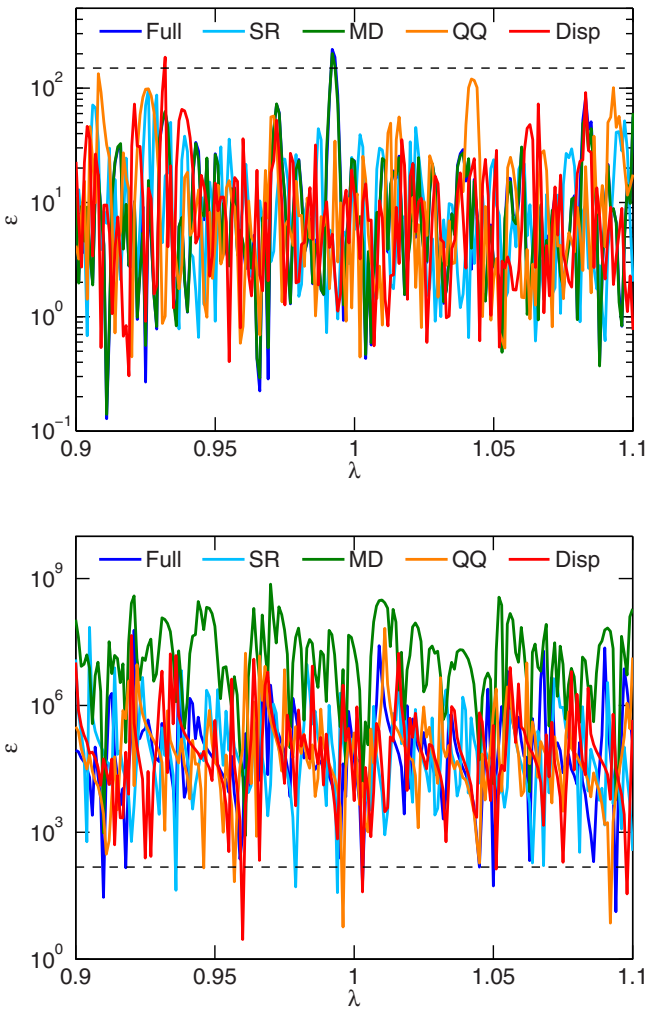

FIG. 5. (Color online) Ratio elastic-to-inelastic, ϵ, as a function of the mass-scaling parameter, λ, for the full calculation (Full) and as obtained when turning off the short-range anisotropy (SR), magnetic dipole coupling (MD), electric quadrupole-quadrupole coupling (QQ), and the dispersion anisotropy (Disp). The dashed horizontal line marks the critical value $\epsilon = 150$. The top and bottom panels show the results for energies of 10^{-3} K and 10^{-6} K, respectively.

scattering calculations with a single anisotropic interaction turned off. We turned off the magnetic dipole-dipole coupling, the long-range electric quadrupole-quadrupole interaction, the long-range dispersion interaction, and the short-range interaction. For the last two interactions, we set the anisotropic components to zero but kept the isotropic terms given by the $k_A = k_B = k_{AB} = 0$ terms in the interaction potential [Eq. (A1)].

Figure 4 shows the elastic and inelastic cross sections as a function of the collision energy. Without the magnetic dipole coupling, the Wigner threshold law continues to suppress the inelastic cross section in the ultracold limit. Thus, turning off the magnetic dipole coupling qualitatively changes the inelastic cross sections in the ultracold regime. Turning off one of the other interactions modifies the scattering resonances and dramatically changes the value of the elastic cross section in the ultracold limit. However, these large differences found in Fig. 4 essentially reflect the sensitivity of the dynamics to the potential, and the variation is comparable to that indicated by the λ scans. This is also shown in Fig. 5, which shows such λ scans with individual anisotropic interactions turned off. At an energy of $E = 10^{-3}$ K, the range in which the ratio of elastic-to-inelastic collisions, ϵ, varies with λ is unaffected by turning off any single anisotropic interaction. At these energies, Zeeman relaxation is driven by both short-ranged and long-ranged anisotropic electronic interactions. At an energy of $E = 10^{-6}$ K, turning off the magnetic dipolar coupling systematically increases the ratio ϵ, as discussed. Thus, the magnetic dipole coupling drives Zeeman relaxation in the ultracold limit for $B = 0$.

V. CONCLUSIONS

A coupled-channels theory description of the scattering dynamics of cold magnetically trapped scandium atoms is presented. We distinguish three regimes. For energies above $E = 10^{-3}$ K the short-range can be reached without a barrier,

and comparable elastic and inelastic scattering cross sections are found. For lower energies, the short range cannot be reached without tunneling through the centrifugal barrier. Therefore, inelastic collisions are suppressed according to the Wigner threshold laws. In the Born regime, for energies below $E = 10^{-6}$ K, tunneling through the centrifugal barrier is so strongly suppressed that magnetic dipolar relaxation in the long range becomes dominant. This relaxation mechanism does not follow the Wigner threshold laws but can be explained in the Born approximation.

Large inelastic cross sections have been found, which is in agreement with experiments with cold submerged-shell atoms. This includes collisions of titanium atoms [37], as well as collisions of the heavier erbium and thulium atoms [4]. In the ultracold regime, the main mechanism for Zeeman relaxation is found to be the magnetic dipolar interaction. Above 10^{-6} K, the relaxation is driven by anisotropic electronic interactions. Below 10^{-4} K, the ratio of elastic-to-inelastic cross sections is likely to be favorable for evaporative cooling.

ACKNOWLEDGMENT

The authors thank Ad van der Avoird for carefully reading the manuscript.

APPENDIX A: MATRIX ELEMENTS IN THE COUPLED BASIS

On the basis of Eq. (12), matrix elements of the interatomic interaction potential are given by Eq. (33) of Ref. [5]. Using $L_A = L'_A = L_B = L'_B = 2$ and $S_A = S'_A = S_B = S'_B = 1/2$, we have

$$\begin{aligned}
&\langle (j_A j_B) j_{AB} \ell; JM | \hat{V}_{\text{elec.}} | (j'_A j'_B) j'_{AB} \ell'; J'M' \rangle \\
&= \delta_{J,J'} \delta_{M,M'} \sum_{S,k_A,k_B,k_{AB}} V^S_{k_A,k_B,k_{AB}}(R) (-1)^{k_A+k_B+j_A+j'_A-j'_{AB}-J-1} [j_A, j'_A, j_B, j'_B, j_{AB}, j'_{AB}, \ell, \ell', k_A, k_B, k_{AB}]^{1/2} [S] \\
&\times \begin{pmatrix} \ell & k_{AB} & \ell' \\ 0 & 0 & 0 \end{pmatrix} \begin{Bmatrix} j_{AB} & j'_{AB} & k_{AB} \\ \ell' & \ell & J \end{Bmatrix} \begin{Bmatrix} k_A & 2 & \frac{1}{2} & \frac{1}{2} & 2 & k_B \\ & & & S & & \\ 2 & j_A & & & j'_B & 2 \\ & & & k_{AB} & & \\ \frac{1}{2} & j'_A & j'_{AB} & j_{AB} & j_B & \frac{1}{2} \end{Bmatrix}. \qquad \text{(A1)}
\end{aligned}$$

Here $[l_1, l_2, \ldots, l_n]$ is a shorthand for $(2l_1+1)(2l_2+1)\cdots(2l_n+1)$, the factor in round brackets a Wigner 3-jm symbol, the quantity in small curly brackets is a Wigner 6-j symbol, and the larger one represents an 18-j symbol, Eq. (A.4.14) of Ref. [33]. The space-fixed expansion of the interaction potential, $V^S_{k_A,k_B,k_{AB}}(R)$, is related to the *ab initio* potential energy surface through Eqs. (6)–(10) and (19) of Ref. [5]. The *ab initio* energy curves are calculated at the NEVPT2/aug-cc-pVQZ level of theory, as reported in the companion paper [11].

The spin-orbit interaction is assumed to be of the form

$$\begin{aligned}
\hat{V}_{SO} &= A_{\text{SO}} (\hat{\mathbf{L}}_{\text{A}} \cdot \hat{\mathbf{S}}_{\text{A}} + \hat{\mathbf{L}}_{\text{B}} \cdot \hat{\mathbf{S}}_{\text{B}}) \\
&= \frac{A_{\text{SO}}}{2} \left(\hat{j}_A^2 - \hat{L}_A^2 - \hat{S}_A^2 + \hat{j}_B^2 - \hat{L}_B^2 - \hat{S}_B^2 \right), \qquad \text{(A2)}
\end{aligned}$$

where A_{SO} is the atomic spin-orbit coupling constant, which has the experimental value of 0.3068 mE_h [20]. This operator is diagonal in the coupled basis, and its matrix elements are

$$\begin{aligned}
&\langle (j_A j_B) j_{AB} \ell; JM | \hat{V}_{SO} | (j'_A j'_B) j'_{AB} \ell'; J'M' \rangle \\
&= \frac{A_{\text{SO}}}{2} \delta_{JJ'} \delta_{MM'} \delta_{jj'} \delta_{\ell\ell'} \delta_{j_a j'_a} \delta_{j_b j'_b} \\
&\times \left[j_A(j_A+1) + j_B(j_B+1) - \frac{27}{2} \right]. \qquad \text{(A3)}
\end{aligned}$$

We now turn to the magnetic interactions. The magnetic dipole moment of each atom is given by Eq. (6). The magnetic dipole-dipole coupling is given by

$$\hat{V}_{\text{magn.dip.}} = -\sqrt{30} \frac{\alpha^2}{R^3} \times \left[[\hat{\boldsymbol{\mu}}_A \otimes \hat{\boldsymbol{\mu}}_B]^{(2)} \otimes C^{(2)}(\hat{R}) \right]^{(0)}_0. \qquad \text{(A4)}$$

Here α is the fine-structure constant, and we define $C^{(2)}(\hat{R})$ to be the rank-2 tensor whose spherical components are Racah normalized spherical harmonics depending on the polar angles of $\hat{R}$ in the space-fixed frame. The symbol

$$[\hat{A}^{(k_A)} \otimes \hat{B}^{(k_B)}]^{(k_{AB})}_{q_{AB}} = \sum_{q_A, q_B} \hat{A}^{(k_A)}_{q_A} \hat{B}^{(k_B)}_{q_B} \langle k_A q_A k_B q_B | k_{AB} q_{AB} \rangle \qquad \text{(A5)}$$

is the spherical component q_{AB} of the irreducible rank-k_{AB} tensor product of $\hat{A}^{(k_A)}$ and $\hat{B}^{(k_B)}$. Note the relation with Eq. (2) of Ref. [29], where the magnetic moment has no orbital contribution. Taking a matrix element, and applying the Wigner-Eckart theorem, we obtain

$$\begin{aligned}
&\langle (j_A j_B) j_{AB} \ell; JM | \hat{V}_{\text{magn.dip.}} | (j'_A j'_B) j'_{AB} \ell'; J'M' \rangle \\
&= -\sqrt{6} \frac{\alpha^2}{R^3} \delta_{JJ'} \delta_{MM'} (-1)^{j'_{AB}+\ell+J} \begin{Bmatrix} j_{AB} & j'_{AB} & 2 \\ \ell' & \ell & J \end{Bmatrix} \\
&\times \langle j_{AB} || [\hat{\boldsymbol{\mu}}_A \otimes \hat{\boldsymbol{\mu}}_B]^{(2)} || j'_{AB} \rangle \langle \ell || C^{(2)} || \ell' \rangle. \qquad \text{(A6)}
\end{aligned}$$

The reduced matrix element of the spherical harmonic is given by

$$\langle \ell || C^{(2)} || \ell' \rangle = (-1)^{\ell} [\ell, \ell']^{1/2} \begin{pmatrix} \ell & 2 & \ell' \\ 0 & 0 & 0 \end{pmatrix}. \qquad \text{(A7)}$$

The other reduced matrix element may be obtained by substituting Eq. (6) for the dipole operator, and subsequently simplified by noting that $\hat{\mathbf{L}}_A$ acts only on $|L_A M_{L_A}\rangle$, and similarly for $\hat{\mathbf{S}}_A$ and atom B. Using for the reduced matrix element of an angular momentum operator

$$\langle j||\hat{\mathbf{j}}||j'\rangle = \delta_{jj'}\sqrt{j(j+1)(2j+1)}, \tag{A8}$$

we have

$$\langle j_{AB}||[\hat{\boldsymbol{\mu}}_A \otimes \hat{\boldsymbol{\mu}}_B]^{(2)}||j'_{AB}\rangle = \sqrt{5}[j_{AB}, j'_{AB}]^{1/2}\langle j_A||\hat{\boldsymbol{\mu}}_A||j'_A\rangle\langle j_B||\hat{\boldsymbol{\mu}}_B||j'_B\rangle \begin{Bmatrix} j_A & j'_A & 1 \\ j_B & j'_B & 1 \\ j_{AB} & j'_{AB} & 2 \end{Bmatrix}, \tag{A9}$$

with

$$\langle j_A||\hat{\boldsymbol{\mu}}_A||j'_A\rangle = \mu_B[j_A, j'_A]^{1/2}(-1)^{1/2}\left[(-1)^{j'_A}\sqrt{30}\begin{Bmatrix} j_A & j'_A & 1 \\ 2 & 2 & \frac{1}{2} \end{Bmatrix} + g_S(-1)^{j_A}\sqrt{3/2}\begin{Bmatrix} j_A & j'_A & 1 \\ \frac{1}{2} & \frac{1}{2} & 2 \end{Bmatrix}\right]. \tag{A10}$$

Proceeding identically for atom B, we obtain

$$\begin{aligned}
&\langle (j_A j_B) j_{AB}\ell; JM|\hat{V}_{\text{magn.dip.}}|(j'_A j'_B) j'_{AB}\ell'; J'M'\rangle \\
&= \delta_{JJ'}\delta_{MM'}\sqrt{30}\frac{(\mu_B\alpha)^2}{R^3}(-1)^{J+j'_{AB}+3/2}[j_A, j'_A, j_B, j'_B, j_{AB}, j'_{AB}, \ell, \ell']^{1/2}\begin{pmatrix} \ell & 2 & \ell' \\ 0 & 0 & 0 \end{pmatrix}\begin{Bmatrix} j_{AB} & j'_{AB} & 2 \\ \ell' & \ell & J \end{Bmatrix}\begin{Bmatrix} j_A & j'_A & 1 \\ j_B & j'_B & 1 \\ j_{AB} & j'_{AB} & 2 \end{Bmatrix} \\
&\times\left[(-1)^{j'_A}\sqrt{30}\begin{Bmatrix} j_A & j'_A & 1 \\ 2 & 2 & \frac{1}{2} \end{Bmatrix} + g_S(-1)^{j_A}\sqrt{3/2}\begin{Bmatrix} j_A & j'_A & 1 \\ \frac{1}{2} & \frac{1}{2} & 2 \end{Bmatrix}\right] \\
&\times\left[(-1)^{j'_B}\sqrt{30}\begin{Bmatrix} j_B & j'_B & 1 \\ 2 & 2 & \frac{1}{2} \end{Bmatrix} + g_S(-1)^{j_B}\sqrt{3/2}\begin{Bmatrix} j_B & j'_B & 1 \\ \frac{1}{2} & \frac{1}{2} & 2 \end{Bmatrix}\right].
\end{aligned} \tag{A11}$$

The interaction with a homogeneous magnetic field is given by

$$\hat{V}_{\text{Zeeman}} = -\hat{\boldsymbol{\mu}}\cdot\vec{B} = \mu_B B(\hat{L}_z + g_s\hat{S}_z), \tag{A12}$$

with the magnetic field, $\vec{B}$, in the space-fixed z direction. The matrix elements of the z component of the angular momentum operators are evaluated using the Wigner-Eckart theorem, for example,

$$\langle (j_A j_B) j_{AB}\ell; JM|\hat{L}_{a,z}|(j'_A j'_B) j'_{AB}\ell'; J'M'\rangle = (-1)^{J-M}\begin{pmatrix} J & 1 & J' \\ -M & 0 & M' \end{pmatrix}\langle (j_A j_B) j_{AB}\ell; J||\hat{\mathbf{L}}_a||(j'_A j'_B) j'_{AB}\ell'; J'\rangle. \tag{A13}$$

Again, the reduced matrix element can be simplified by noting that $\hat{\mathbf{L}}_A$ acts only on $|L_A M_{L_A}\rangle$. Proceeding identically for $\hat{\mathbf{S}}_A$ and the second atom, combining the results yields

$$\begin{aligned}
&\langle (j_A j_B) j_{AB}\ell; JM|\hat{V}_{\text{Zeeman}}|(j'_A j'_B) j'_{AB}\ell'; J'M'\rangle \\
&= (-1)^{J-M+j_{AB}+J'+\ell+j_A+3/2}\delta_{\ell\ell'}\mu_B B[J, J', j_{AB}, j'_{AB}]^{1/2}\begin{pmatrix} J & 1 & J' \\ -M & 0 & M' \end{pmatrix}\begin{Bmatrix} J & J' & 1 \\ j'_{AB} & j_{AB} & \ell \end{Bmatrix} \\
&\times\left[\delta_{j_B j'_B}(-1)^{j_B+j'_{AB}+j'_A}[j_A, j'_A]^{1/2}\sqrt{30}\begin{Bmatrix} j_{AB} & j'_{AB} & 1 \\ j'_A & j_A & j_B \end{Bmatrix}\begin{Bmatrix} j_A & j'_A & 1 \\ 2 & 2 & \frac{1}{2} \end{Bmatrix}\right. \\
&+\delta_{j_A j'_A}(-1)^{j'_B+j_{AB}+j'_B}[j_B, j'_B]^{1/2}\sqrt{30}\begin{Bmatrix} j_{AB} & j'_{AB} & 1 \\ j'_B & j_B & j_A \end{Bmatrix}\begin{Bmatrix} j_B & j'_B & 1 \\ 2 & 2 & \frac{1}{2} \end{Bmatrix} \\
&+g_s\delta_{j_B j'_B}(-1)^{j_B+j'_{AB}+j_A}[j_A, j'_A]^{1/2}\sqrt{3/2}\begin{Bmatrix} j_{AB} & j'_{AB} & 1 \\ j'_A & j_A & j_B \end{Bmatrix}\begin{Bmatrix} j_A & j'_A & 1 \\ \frac{1}{2} & \frac{1}{2} & 2 \end{Bmatrix} \\
&\left.+\ g_s\delta_{j_A j'_A}(-1)^{j'_B+j_{AB}+j_B}[j_B, j'_B]^{1/2}\sqrt{3/2}\begin{Bmatrix} j_{AB} & j'_{AB} & 1 \\ j'_B & j_B & j_A \end{Bmatrix}\begin{Bmatrix} j_B & j'_B & 1 \\ \frac{1}{2} & \frac{1}{2} & 2 \end{Bmatrix}\right].
\end{aligned} \tag{A14}$$

APPENDIX B: SYMMETRY OPERATIONS

In this Appendix we consider the action of symmetry operators on the channel functions [Eq. (12)]. In particular, we consider spatial inversion and the permutation of identical nuclei.

Following Ref. [38], we write the channel functions explicitly as

$$\begin{aligned}|(j_A j_B)j_{AB}\ell; JM\rangle = \hat{\mathcal{A}} \sum_{m_A,m_B,m_{AB},m_\ell} & \Phi_{L_A,S_A,j_A,m_A}\left(\vec{r}_1-\vec{R}_A,\omega_1,\vec{r}_2-\vec{R}_A,\omega_2,\ldots,\vec{r}_{n_e}-\vec{R}_A,\omega_{n_e}\right)\\ &\times \Phi_{L_B,S_B,j_B,m_B}\left(\vec{r}_{n_e+1}-\vec{R}_B,\omega_{n_e+1},\vec{r}_{n_e+2}-\vec{R}_B,\omega_{n_e+2},\ldots,\vec{r}_{n_e+n_e}-\vec{R}_B,\omega_{n_e+n_e}\right)\\ &\times |\ell m_\ell\rangle\langle j_A m_A j_B m_B|j_{AB}m_{AB}\rangle\langle j_{AB}m_{AB}\ell m_\ell|JM\rangle,\end{aligned} \tag{B1}$$

with $\vec{r}_i$ the spatial coordinates of electron i, ω_i denotes the electron spin coordinates $n_e = 21$ is the number of electrons of the scandium atom, and R_X the coordinates of nucleus X with $X = A,B$. Denoted by $\Phi_{L,S,j,m}(\vec{r}_1,\omega_1\vec{r}_2,\omega_2,\ldots,\vec{r}_{n_e},\omega_{n_e})$ is the electronic wave function of an atom at the origin, with orbital (L) and spin (S) electronic angular momentum, which are coupled to a total, j, with space-fixed projection quantum number m. The operator $\hat{\mathcal{A}}$ antisymmetrizes the wave function with respect to the interchange of any two electrons. We note that, strictly speaking, the transformed adiabatic states are written as products of atomic states only for asymptotically large R. However, the symmetry properties derived in this section are the same for finite and asymptotically large R.

The spatial inversion operator, $\hat{\imath}$, inverts the coordinates of all particles with respect to the center of mass of the dimer,

$$\begin{aligned}\hat{\imath}\vec{r}_i\hat{\imath}^\dagger &= -\vec{r}_i,\\ \hat{\imath}\vec{R}_A\hat{\imath}^\dagger &= -\vec{R}_A = \vec{R}_B,\end{aligned} \tag{B2}$$

The electronic wave functions have well-defined parity, which is *gerade* in the case of scandium, whereas the nuclear wave function obtains a phase $(-1)^\ell$ under inversion. Thus, the coupled space-fixed functions of Eq. (12) have definite parity given by $(-1)^\ell$, as they transform under inversion as

$$\hat{\imath}|(j_A j_B)j_{AB}\ell; JM\rangle = (-1)^\ell|(j_A j_B)j_{AB}\ell; JM\rangle. \tag{B3}$$

We denote the operator that interchanges the two identical nuclei by $\hat{P}_{AB}$. The action of the permutation operator on the coordinates of the particles is given by

$$\begin{aligned}\hat{P}_{AB}\vec{r}_i\hat{P}_{AB}^\dagger &= \vec{r}_i,\\ \hat{P}_{AB}\vec{R}_A\hat{P}_{AB}^\dagger &= \vec{R}_B.\end{aligned} \tag{B4}$$

The action of $\hat{P}_{AB}$ on the nuclear wave function is identical to inversion of the nuclear coordinates, which yields a phase of $(-1)^\ell$. The permutation operator, $\hat{P}_{AB}$, does not act on the electronic coordinates in the space-fixed frame. However, the electronic wave function of atom A is centered at $\vec{R}_A$, hence it parametrically depends on $\vec{R}_A$. Under the action of $\hat{P}_{AB}$, we obtain for the electronic part

$$\begin{aligned}&\hat{P}_{AB}\hat{\mathcal{A}}\Phi_{\gamma_A}(1,2,\ldots,n_e;R_A)\Phi_{\gamma_B}(n_e+1,n_e+2,\ldots,n_e+n_e;R_B)\\ &\quad=\hat{\mathcal{A}}\Phi_{\gamma_A}(1,2,\ldots,n_e;R_B)\Phi_{\gamma_B}(n_e+1,n_e+2,\ldots,n_e+n_e;R_A)\\ &\quad=\hat{\mathcal{A}}\hat{\mathcal{P}}\Phi_{\gamma_A}(n_e+1,n_e+2,\ldots,n_e+n_e;R_B)\Phi_{\gamma_B}(1,2,\ldots,n_e;R_A)\\ &\quad=(-1)^{n_e}\hat{\mathcal{A}}\Phi_{\gamma_B}(1,2,\ldots,n_e;R_A)\Phi_{\gamma_A}(n_e+1,n_e+2,\ldots,n_e+n_e;R_B),\end{aligned} \tag{B5}$$

where $\Phi_{\gamma_A}(1,2,\ldots,n_e;R_A)$ is a shorthand notation for $\Phi_{L_A,S_A,j_A,m_A}(\vec{r}_1-\vec{R}_A,\omega_1,\vec{r}_2-\vec{R}_A,\omega_2,\ldots,\vec{r}_{n_e}-\vec{R}_A,\omega_{n_e})$. The permutation operator $\hat{\mathcal{P}}$ interchanges electrons i and $i+n_e$ for all $i\in\{1,2,\ldots,n_e\}$, and in the last step we used $\hat{\mathcal{A}}\hat{\mathcal{P}} = (-1)^p\hat{\mathcal{A}}$, where p is the parity of the permutation operator, $\hat{\mathcal{P}}$, which equals n_e.

Combining the results above, and using

$$\langle j_A m_A j_B m_B|j_{AB}m_{AB}\rangle = (-1)^{j_A+j_B-j_{AB}}\langle j_B m_B j_A m_A|j_{AB}m_{AB}\rangle, \tag{B6}$$

we have for the action of $\hat{P}_{AB}$ on the channel functions

$$\hat{P}_{AB}|(j_A j_B)j_{AB}\ell; JM\rangle = (-1)^{j_A+j_B-j_{AB}+\ell+n_e}|(j_B j_A)j_{AB}\ell; JM\rangle. \tag{B7}$$

[1] C. C. Bradley, C. A. Sackett, J. J. Tollett, and R. G. Hulet, Phys. Rev. Lett. **75**, 1687 (1995).

[2] M. H. Anderson, J. R. Ensher, M. R. Matthews, C. E. Wieman, and E. A. Cornell, Science **269**, 198 (1995).

[3] K. B. Davis, M.-O. Mewes, M. R. Andrews, N. J. van Druten, D. S. Durfee, D. M. Kurn, and W. Ketterle, Phys. Rev. Lett. **75**, 3969 (1995).
[4] C. B. Connolly, Y. S. Au, S. C. Doret, W. Ketterle, and J. M. Doyle, Phys. Rev. A **81**, 010702 (2010).
[5] R. V. Krems, G. C. Groenenboom, and A. Dalgarno, J. Phys. Chem. A **108**, 8941 (2004).
[6] C. I. Hancox, S. C. Doret, M. T. Hummon, L. Luo, and J. M. Doyle, Nature (London) **431**, 281 (2004).
[7] J. G. E. Harris, S. V. Nguyen, S. C. Doret, W. Ketterle, and J. M. Doyle, Phys. Rev. Lett. **99**, 223201 (2007).
[8] R. V. Krems, J. Kłos, M. F. Rode, M. M. Szczesniak, G. Chałasinski, and A. Dalgarno, Phys. Rev. Lett. **94**, 013202 (2005).
[9] M.-J. Lu, K. S. Hardman, J. D. Weinstein, and B. Zygelman, Phys. Rev. A **77**, 060701 (2008).
[10] B. Zygelman and J. D. Weinstein, Phys. Rev. A **78**, 012705 (2008).
[11] T. Karman, X. Chu, and G. C. Groenenboom, preceding paper, Phys. Rev. A **90**, 052701 (2014).
[12] V. Kokoouline, R. Santra, and C. H. Greene, Phys. Rev. Lett. **90**, 253201 (2003).
[13] R. Santra and C. H. Greene, Phys. Rev. A **67**, 062713 (2003).
[14] S. H. Lipoff and D. R. Herschbach, Mol. Phys. **108**, 1133 (2010).
[15] S. Kotochigova and A. Petrov, Phys. Chem. Chem. Phys. **13**, 19165 (2011).
[16] A. Petrov, E. Tiesinga, and S. Kotochigova, Phys. Rev. Lett. **109**, 103002 (2012).
[17] T. V. Tscherbul, A. A. Buchachenko, A. Dalgarno, M.-J. Lu, and J. D. Weinstein, Phys. Rev. A **80**, 040701 (2009).
[18] C. B. Connolly, Y. S. Au, E. Chae, T. V. Tscherbul, A. A. Buchachenko, H.-I. Lu, W. Ketterle, and J. M. Doyle, Phys. Rev. Lett. **110**, 173202 (2013).
[19] G. C. Groenenboom, X. Chu, and R. V. Krems, J. Chem. Phys. **126**, 204306 (2007).
[20] J. Sugar and C. Corliss, J. Phys. Chem. Ref. Data **14**, 1 (1985).
[21] B. Zygelman, A. Dalgarno, and R. D. Sharma, Phys. Rev. A **49**, 2587 (1994).
[22] B. R. Johnson, NRCC Proc. **5**, 86 (1979).
[23] T. Karman, L. M. C. Janssen, R. Sprenkels, and G. C. Groenenboom, J. Chem. Phys. **141**, 064102 (2014).
[24] M. Abramowitz and I. A. Stegun, *Handbook of Mathematical Functions* (National Bureau of Standards, Washington, DC, 1964).
[25] L. M. C. Janssen, P. S. Żuchowski, A. van der Avoird, G. C. Groenenboom, and J. M. Hutson, Phys. Rev. A **83**, 022713 (2011).
[26] E. P. Wigner, Phys. Rev. **73**, 1002 (1948).
[27] H. R. Sadeghpour, J. L. Bohn, M. J. Cavagnero, B. D. Esry, I. I. Fabrikant, J. H. Macek, and A. R. P. Rau, J. Phys. B **33**, R93 (2000).
[28] R. V. Krems, A. Dalgarno, N. Balakrishnan, and G. C. Groenenboom, Phys. Rev. A **67**, 060703 (2003).
[29] L. M. C. Janssen, P. S. Żuchowski, A. van der Avoird, J. M. Hutson, and G. C. Groenenboom, J. Chem. Phys. **134**, 124309 (2011).
[30] A. Volpi and J. L. Bohn, Phys. Rev. A **65**, 052712 (2002).
[31] MATLAB Version 6, http://www.mathworks.com
[32] See Supplemental Material at http://link.aps.org/supplemental/10.1103/PhysRevA.90.052702 for the Born approximation and for coupled-channels code.
[33] A. P. Yutsis, I. B. Levinson, and V. V. Vanagas, *Mathematical Apparatus of the Theory of Angular Momentum* (Israel Program for Scientific Translations, Jerusalem, 1962).
[34] C. R. Monroe, E. A. Cornell, C. A. Sackett, C. J. Myatt, and C. E. Wieman, Phys. Rev. Lett. **70**, 414 (1993).
[35] J. D. Weinstein, R. deCarvalho, T. Guillet, B. Friedrich, and J. M. Doyle, Nature (London) **395**, 148 (1998).
[36] P. S. Żuchowski and J. M. Hutson, Phys. Chem. Chem. Phys. **13**, 3669 (2011).
[37] M.-J. Lu, V. Singh, and J. D. Weinstein, Phys. Rev. A **79**, 050702 (2009).
[38] Elementary Derivation of Some of the Wigner-Witmer Rules, P. Pechukas and R. N. Zare, Am. J. Phys. **40**, 1687 (1972).